Magn Reson Mater Phy (2011) 24:127–135
DOI 10.1007/s10334-010-0242-7

RESEARCH ARTICLE

SAR reduced black-blood cine TPM for increased temporal resolution at 3T

Anja Lutz · Axel Bornstedt · Robert Manzke · G. Ulrich Nienhaus · Patrick Etyngier · Volker Rasche

Received: 6 September 2010 / Revised: 21 December 2010 / Accepted: 22 December 2010 / Published online: 19 January 2011

Abstract
Object The objective was to improve the temporal resolution in black-blood CINE tissue phase mapping sequences at high field MR systems. The temporal resolution is limited due to SAR constraints causing idle times into the sequence. The aim was to avoid these idle times and therefore providing an increased number of heart phases.
Materials and methods Thirteen volunteers were enrolled in this study. Each volunteer underwent different myocardial short-axis scans comprising scans with application of both presaturation pulses, with alternating application of presaturation pulses and with an attenuation of the excitation angle. The last two approaches enable a SAR reduction or increased temporal resolution. The contrast to noise ratio (CNR) between myocardium and blood and the influence on the measured tissue motion were investigated.
Results High CNR between myocardium and blood could be obtained with the application of alternating presaturation-pulses. Reduction of the flip angle of the presaturation-pulses provided reduced CNR relative to both the original and the alternated presaturation-pulses approach. More details of the myocardial motion were observed with increased temporal resolution.
Conclusion It is feasible to increase the temporal resolution at high field strength by reducing the SAR with either alternating presaturation-pulses or decreased flip angle of these pulses.

Keywords Tissue phase mapping · High field strength · Black-blood · Temporal resolution

A. Lutz (✉) · A. Bornstedt · V. Rasche
University Hospital of Ulm, Albert-Einstein-Allee 23, 89081 Ulm, Germany
e-mail: Anja.Lutz@uniklinik-ulm.de

R. Manzke
Philips Research North America, Briarcliff Manor, NY, USA

G. U. Nienhaus
Karlsruhe Institute of Technology (KIT), Karlsruhe, Germany

P. Etyngier
Medisys Research Lab, Philips Healthcare, Suresnes, France

Introduction

In cardiac tissue phase mapping (TPM), black-blood contrast is preferred to avoid flow-related phase errors superimposed on the quantitative myocardial phase information and to improve the delineation between myocardium and blood pool [1–5].

Several techniques have been introduced for establishing black-blood contrast. These methods comprise spatial presaturation [2,6,7], 180° RF refocusing pulses [8], inversion recovery (IR) and double inversion recovery (DIR) approaches [9,10], susceptibility weighted imaging (SWI) [11], the application of stimulated echo techniques (STEAM) [12–15], and motion sensitizing (MS) for blood signal suppression [16–19].

Due to the temporal resolution demands in cine imaging, SWI and IR-based methods are not applicable to black-blood TPM. The application of STEAM and MS to TPM imaging appears possible but is limited by the concomitant signal reduction in the moving myocardium especially in phases of rapid motion, as already shown in the black-blood SSFP sequence developed on the basis of STEAM by Basha et al. [15]. Here, a considerable B_0 field inhomogeneity within the myocardium was observed, which was attributed to the deformation of the heart. More promising for achieving black-blood contrast in TPM appear a spin-echo preparation

[8] or presaturation of spins adjacent to the imaged slice [2,6,7]. Both approaches rely on an almost complete blood exchange between the spin preparation and the actual measurement. In the presaturation technique, either two subsequent presaturation pulses adjacent to the imaged slice [6] or a sandwich-pulse [7] have been introduced. Since the presaturation techniques do not compromise myocardial signal in the imaged slice and can be implemented efficiently, they appear to be the most promising techniques for achieving black-blood contrast in TPM.

However, due to specific absorption rate (SAR) constraints, idle times have to be introduced into the black-blood cine TPM sequence at high field MR systems, thus causing a reduction of the maximal number of measurable cardiac phases in the TPM acquisition. Left ventricular functional analysis requires adequate high temporal resolution and hence a high number of cardiac phases [20,21] to ensure assessment of all details of the myocardial contraction pattern [22,23] and to avoid a reduction of the peak velocities [23]. In [20,21] the influence on the temporal resolution for important functional parameters is investigated. The end-diastolic volume (EDV) and left ventricular mass show no significant variations, whereas the ejection fraction (EF) decreases with increasing frame duration (significant for frame durations longer than 45 ms). A comparison of different temporal resolutions in black-blood CINE TPM data was performed by Jung et al. [23]. He showed, that a high temporal resolution of 13.8 ms results in higher radial diastolic peak velocities than a low temporal resolution of 69 ms. From these data it can be conducted that a minimal temporal resolution of 45 ms is required for adequate assessment of the myocardial motion. On high field MRI systems a reduction of SAR appears mandatory for ensuring sufficient temporal resolution in TPM imaging.

It is the objective of this study to investigate different SAR reduction schemes regarding their potential for improving the temporal resolution in TPM imaging. Two approaches have been investigated: (a) reduction of the flip angle of the presaturation pulses and (b) alternating application of the two presaturation pulses with 90° flip angle. Both approaches enable an improved temporal resolution and a more detailed assessment of quantitative myocardial velocities compared to the standard black-blood acquisition at high field strengths.

Materials and methods

Volunteers

A total of 13 volunteers (6 females, 7 males, age 25 ± 4 years) were enrolled in this study. The study protocol was approved by the local ethics committee. All volunteers provided written informed consent prior to the MRI examination.

Data acquisition

Image acquisition was performed on a 3T whole body MR scanner (Achieva 3.0T, Philips, Best, The Netherlands) with a 32 [$2 \times 4 \times 4$] channel phased array cardiac coil.

After the rapid survey, a coil-sensitivity reference scan was acquired, which was needed for the vendor specific homogenization of the image signals produced by the 32 coil elements. Breathhold cine cardiac two-chamber and four-chamber views were acquired to define the central short-axis image orientation, which was used in all subsequent acquisitions.

The TPM acquisition was performed applying a black blood prepared, respiratory navigated, segmented and velocity encoded cardiac triggered gradient echo sequence. The acquisition parameters were: TE/TR = 4.7 ms/7 ms, flip angle = 15°, resolution = $2 \times 2 \times 8\,\text{mm}^3$, 3 k-lines/segment, acquisition matrix ($M \times P$) = 172×168. The acquisition window was 90% of the RR-interval. Isotropic velocity encoding of 30 cm/s was performed in a Hadamard fashion by a balanced four-point velocity vector method thus using linear combinations of velocity encoding in all three directions simultaneously [24–26]. To improve the temporal resolution, velocity encoding was performed in an interleaved fashion, so that different velocity-encoding steps were acquired in subsequent heart cycles [27].

Two presaturation slabs adjacent to the imaged slice [2,3,6] were applied for black-blood preparation. Each presaturation slab was 40 mm thick and placed at 12 mm distance to the imaged slice. The presaturation module was 12 ms long, consisting of two presaturation pulses with 4.6 ms duration each and 2.8 ms long spoiler gradients. The presaturation pulses had a maximum-phase SLR pulse shape. For respiratory motion compensation, conventional navigator-gating and tracking with an acceptance window of 10 mm was performed applying a pencil beam navigator through the dome of the right hemi-diaphragm [28]. The navigator was applied at each start of the cardiac cycle [29]. Cardiac triggering was achieved using a vector electrocardiogram.

To acquire a maximal number of heart phases the B1-amplitude was optimized to 8 μT in all experiments. Further reducing the B1-amplitude prolonged the presaturation pulse part of the sequence, whereas higher B1-amplitudes resulted in prolonged idle times.

In each volunteer, the following sequences with different SAR demands were evaluated (see Fig. 1):

– $\text{DS}^{n_{\text{DS}}}$: two saturation slabs next to the imaged slice and best achievable associated temporal resolution. DS refers to dual saturation and n_{DS} to the maximum number of heart phases measurable with dual saturation. In this sequence both presaturation pulses were applied before each heart phase with a flip angle $\alpha_{\text{presat}} = 90°$.

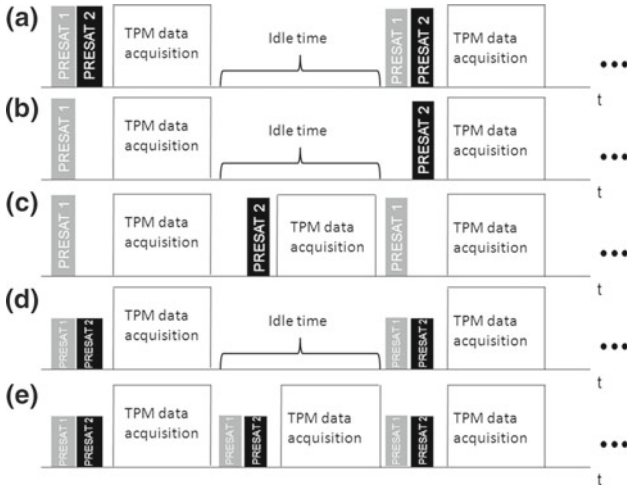

Fig. 1 Schema of the investigated sequences. Schema of the investigated sequences **a** $DS^{n_{DS}}$, **b** $AS^{n_{DS}}$, **c** $AS^{n_{AS}}$, **d** $RF^{n_{DS}}$ and **e** $RF^{n_{AS}}$. In the sequence $DS^{n_{DS}}$ two saturation slabs next to the imaged slice were applied before each heart phase. Idle times were introduced due to SAR limits. In the sequences $AS^{n_{DS}}$ and $AS^{n_{AS}}$ the presaturation pulses were applied in an alternating mode. In the sequences $RF^{n_{DS}}$ and $RF^{n_{AS}}$ the flip angle of the presaturation pulses was reduced to 52°. In the sequences $AS^{n_{DS}}$ and $RF^{n_{DS}}$ idle times were introduced in order to allow a fair comparison to the conventional approach. In the sequences $AS^{n_{AS}}$ and $RF^{n_{AS}}$ the number of heart phases was increased to n_{AS}

- $AS^{n_{DS}}$: two saturation slabs applied in an alternating mode, such that only a single presaturation pulse was applied before each heart phase ($\alpha_{presat} = 90°$). The sequence was measured with n_{DS} heart phases in order to allow a fair comparison to the conventional approach.
- $AS^{n_{AS}}$: alternating saturation pulses acquired with the maximum number of heart phases n_{AS} possible with alternating saturation.
- $RF^{n_{AS}}$: dual saturation, but with a reduced presaturation flip angle of 52°, which allowed the same number of maximum phases n_{AS} as in the alternating presaturation pulses approach.
- $RF^{n_{DS}}$: dual saturation with a reduced flip angle of 52° and n_{DS} number of heart phases.

Data analysis

The TPM MR images were analyzed by an in-house developed MATLAB software (R2008a; Mathworks, Natick, MA). The segmentation of the myocardium was performed automatically relying on active contour techniques by incorporating a shape model. After the segmentation of the first phase, the information was propagated through the entire sequence by tracking profile intensities [30,31].

The blood pool was defined as the area inside the detected endocardial border. The papillary muscles were removed from the blood pool mask using a threshold algorithm:

$$\{I_{\text{blood}}\} = \{I | I \leq \bar{I}_{\text{myo}} - 2\sigma_{I_{\text{myo}}}\}, \tag{1}$$

with I_{blood} describing the intensity of blood, $\bar{I}_{\text{myo}}$ describing the mean intensity of the myocardium and $\sigma_{I_{\text{myo}}}$ being the standard deviation of I_{myo}. The contrast to noise ratio CNR of each heart phase was calculated as

$$\text{CNR}_{\text{ph}} = \frac{|\bar{I}_{\text{myo}} - \bar{I}_{\text{blood}}|}{\sigma_I}, \quad \text{with} \quad \sigma_I = \frac{\sigma_{I_{\text{myo}}} + \sigma_{I_{\text{blood}}}}{2}, \tag{2}$$

where $\bar{I}_{\text{blood}}$ is the mean intensity of the blood and σ_I is the standard deviation. $\sigma_{I_{\text{blood}}}$ denotes the standard deviation of the blood. A mean CNR value over all heart phases was calculated as:

$$\text{CNR} = \frac{1}{n} \sum_{\text{ph}=1}^{n} \text{CNR}_{\text{ph}} \tag{3}$$

where n was the number of heart phases. For the above described five sequences, the CNR was calculated in all volunteers and the mean value $\overline{\text{CNR}}$ and standard deviation σ_{CNR} of CNR over all volunteers were determined. Additionally, the maximum and minimum values of CNR_{ph} (CNR_{max} and CNR_{min}) and the respective mean values $\overline{\text{CNR}}_{\text{max}}$ and $\overline{\text{CNR}}_{\text{min}}$ over all volunteers were calculated.

For investigation of spatially varying saturation effects, the CNR was separately determined for the septal and lateral part of the left ventricle. The mean values $\overline{\text{CNR}}_{\text{sep}}$ and $\overline{\text{CNR}}_{\text{lat}}$ over all volunteers were calculated. For the evaluation of temporal varying saturation effects over the cardiac cycle, the CNR of defined time steps of the RR-interval was calculated by interpolation of CNR_{ph} over time for each volunteer. These CNR values are denoted as CNR_p, where p defines the percentage of RR-interval. Afterward, the mean value and standard deviation of CNR_p over all volunteers were determined for all sequences. A two-tailed paired t test was performed to evaluate the statistical significance with P values below 0.05 being considered significant.

Before quantification of the resulting myocardial velocities, a background phase error correction was performed using a linear fit to the phase of static tissue as suggested earlier [32]. The radial (toward the center of the blood pool) and longitudinal (toward the apex of the heart) velocity curves were calculated. Velocity–time curves for either direction of motion were generated using the average myocardial velocity of the respective imaged slice. Prior to the analysis the velocity data acquired over time were interpolated by cubic splines to provide a continuous velocity profile and to allow comparison of sequences with a different number of sampled heart phases. Physiologically, the accumulated phase over the entire heart cycle must result

to zero. To compensate for nonlinear phase error contributions, in a subsequent correction step the resulting velocity curves were shifted accordingly to meet the physiological conditions.

To evaluate the impact of the different presaturation approaches on the measured velocity information, the correlation coefficient r(sequence x, sequence y) between the velocity curves obtained without and with SAR reduction were calculated for radial and longitudinal velocity measurements. Additionally, the radial and longitudinal velocity range $\Delta v = v_{max} - v_{min}$ was calculated for each sequence and each volunteer. The mean velocity ranges over all volunteers were determined. In healthy volunteers, high resolution analysis of radial and longitudinal myocardial motion reveals two main minima (one local at end-systole and one global) in the equatorial slice [22]. Therefore, the percentage of detected local minima at end-systole over all volunteers P_{local} is determined for both radial and longitudinal motion directions.

Results

The nominal scan duration of each sequence, which describes the acquisition time with 100% navigator acceptance, resulted to 3:45 min. The regular navigator acceptance was in the range of 30–70%, thus resulting in total scan durations between 5:35 and 12:30 min. The duration of a single k-space segment was 40 ms, comprising the presaturation pulse (12 ms) and the acquisition of 3 k-space lines with a single start-up excitation (28 ms).

For a cardiac frequency of 60 beats per minute, the temporal resolution was 68 ms for $n_{DS} = 13$ heart phases and 40 ms for $n_{AS} = 22$ heart phases, indicating an introduced idle time of 28 ms per phase due to SAR limitations in the conventional technique.

The average beats per minute over all volunteers was 70 ± 8. The maximum n_{DS} /n_{AS} across all subjects resulted to 13/21, the minimum n_{DS} /n_{AS} to 10/16.

For n_{DS} heart phases, SAR was reduced to ≈52% compared to the $DS^{n_{DS}}$ sequence for the alternating application of presaturation pulses and to ≈61% for the reduced presaturation flip angle approach. The different techniques and their features are listed in Table 1.

Figure 2 summarizes the resulting black-blood images at end-diastole obtained by the different approaches exemplary for one volunteer. Visual inspection suggested best performance of the conventional technique $DS^{n_{DS}}$ followed by the approach of alternating application of presaturation pulses $AS^{n_{AS}}$. Least suppression of blood was obtained by the reduced flip angle approach $RF^{n_{DS}}$ with n_{DS} heart phases. The visual impression was confirmed by the quantitative analysis (Fig. 3).

$DS^{n_{DS}}$ resulted in maximum $\overline{CNR}$. $AS^{n_{DS}}$ and $AS^{n_{AS}}$ resulted in significant higher $\overline{CNR}$ than $RF^{n_{DS}}$ (P-value ($AS^{n_{DS}}$, $RF^{n_{DS}}$) ≤ 0.01) and $RF^{n_{AS}}$ (P-value($AS^{n_{AS}}$, $RF^{n_{AS}}$) ≤ 0.01). For both, the alternating application and the reduced flip angle approach the $\overline{CNR}$ values obtained with n_{AS} number of heart phases were higher than those obtained with n_{DS} heart phases. For the alternating approach, this difference was significant (P-value = 0.01), whereas for the reduced flip angle approach this difference was not significant (P-value = 0.08). For all but the $\overline{CNR}$ value obtained with the sequence $AS^{n_{AS}}$, the CNR reduction was significant (Fig. 3). For $\overline{CNR}_{max}$, no significant difference was observed for the alternated approach compared to the values obtained with the conventional technique. For $\overline{CNR}_{min}$, a nonsignificant difference was only observed for the sequence $AS^{n_{AS}}$. For all but the $AS^{n_{AS}}$ sequence at least one of the values $\overline{CNR}$, $\overline{CNR}_{max}$ or $\overline{CNR}_{min}$ was significantly reduced. Relative CNR losses ranged from 2 to 6% for $\overline{CNR}$, from 0 to 3% for $\overline{CNR}_{max}$ and from 2 to 5% for $\overline{CNR}_{min}$.

Figure 3 shows the values $\overline{CNR}_{sep}$ and $\overline{CNR}_{lat}$. For the septum significant $\overline{CNR}_{sep}$ reduction compared to $DS^{n_{DS}}$ was only observed for $AS^{n_{DS}}$ and $RF^{n_{DS}}$. For $\overline{CNR}_{lat}$ no significant reduction was obtained.

Figure 4 shows the values CNR_p for $p = n*10\%$, where n are integers between 1 and 9. Less CNR was obtained in heart phases, where blood exchange is limited. At all but one point

Table 1 Parameters of presaturation pulses for the five different techniques $DS^{n_{DS}}$, $AS^{n_{DS}}$, $AS^{n_{AS}}$, $RF^{n_{DS}}$ and $RF^{n_{AS}}$. n_{ph} denotes the measured heart phases

Technique	Alternating presaturation	Flip angle (°)	n_{ph}	SAR (%)	SR (%)	Temp. resolution (ms)	Idle time/phase (ms)
$DS^{n_{DS}}$	No	90	13	90	100	68	28
$AS^{n_{DS}}$	Yes	90	13	47	52.2	68	28
$AS^{n_{AS}}$	Yes	90	21	77	85.6	40	0
$RF^{n_{DS}}$	No	52	13	55	61.1	68	28
$RF^{n_{AS}}$	No	52	21	89	98.9	40	0

SR is the SAR reduction compared to the conventional sequence SR $= \frac{SAR(seq.)}{SAR(DS^{n_{DS}})} \cdot 100\%$. All parameters listed are for a heart frequency of 60 beats per minute

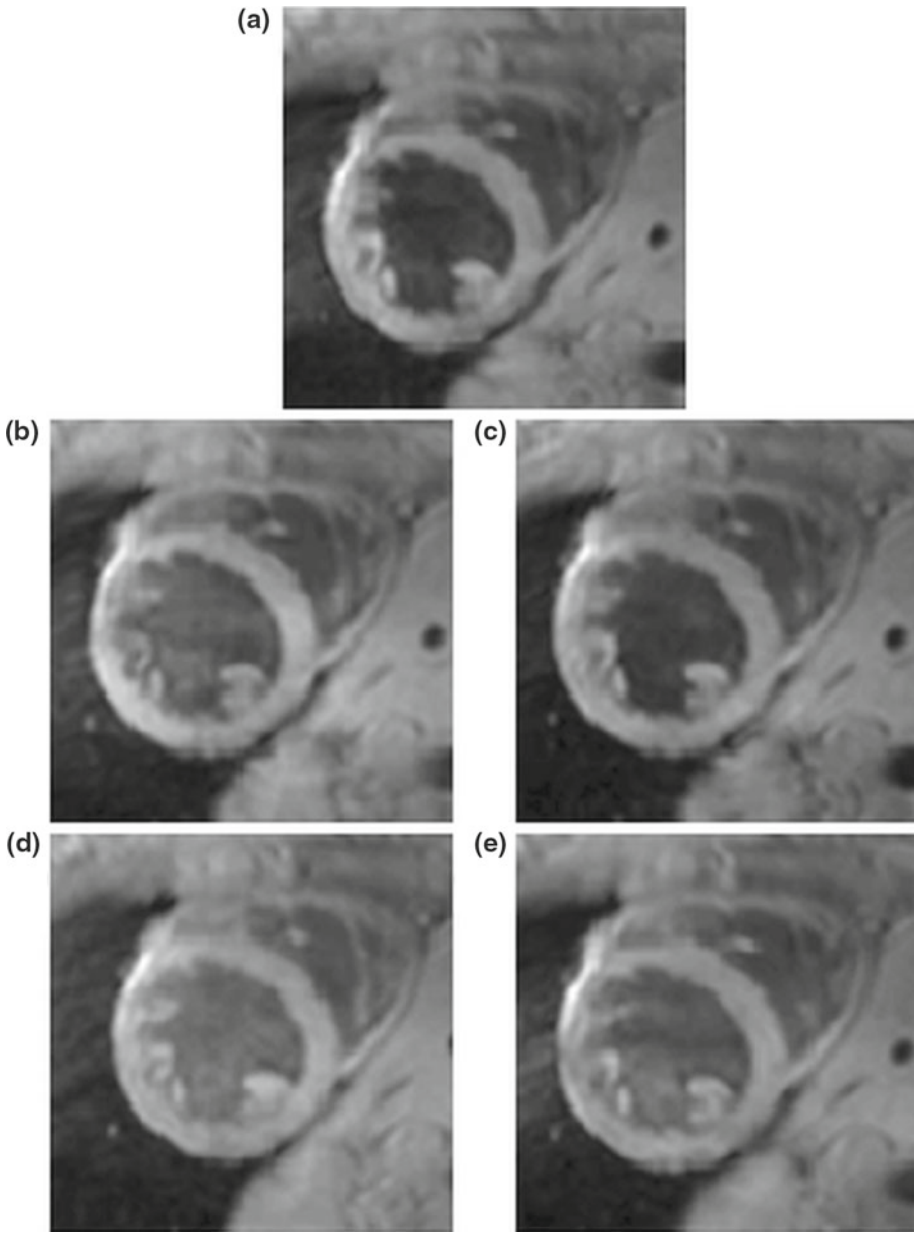

Fig. 2 TPM black-blood images acquired by the investigated sequences exemplary for one volunteer. TPM black-blood images at end-diastole acquired by the sequences **a** $DS^{n_{DS}}$, **b** $AS^{n_{DS}}$, **c** $AS^{n_{AS}}$, **d** $RF^{n_{DS}}$ and **e** $RF^{n_{AS}}$ exemplary for one volunteer. Visual inspection suggested best performance for $DS^{n_{DS}}$ followed by $AS^{n_{AS}}$. Least suppression of blood was obtained by the reduced flip angle approach $RF^{n_{DS}}$

in time, the best CNR_p was obtained by $DS^{n_{DS}}$, followed by $AS^{n_{AS}}$. Although there is a clear trend to improved CNR in $DS^{n_{DS}}$, statistically significant differences between $DS^{n_{DS}}$ and $AS^{n_{AS}}$ were only observed for $CNR_{10\%}$ and $CNR_{20\%}$ (P-values ≤ 0.05). $RF^{n_{DS}}$, $RF^{n_{AS}}$ and $AS^{n_{DS}}$ show significant lower CNR_p for most cardiac phases.

Figure 5 displays the radial velocities obtained by the five sequences exemplarily for one volunteer. The low temporal resolution sequences resulted in slightly reduced diastolic peak velocity values of the diastolic relaxations compared to the high temporal resolution sequences. Additionally, more details were seen in the velocity values obtained with the high temporal resolution sequences (for example a small peak at approximately 420 ms).

The values of the correlation coefficient r(sequence x, sequence y) (Table 2) were all higher than 0.94 thus showing a good agreement between the general shape of the motion curves. The correlation coefficients for the high temporal resolution sequences $r(DS^{n_{DS}}, AS^{n_{AS}})$ and $r(DS^{n_{DS}}, RF^{n_{AS}})$ were lower than the coefficients $r(DS^{n_{DS}}, AS^{n_{DS}})$ and $r(DS^{n_{DS}}, RF^{n_{DS}})$. The radial and longitudinal velocity ranges are listed in Table 2. For both motion directions, the sequences with higher temporal resolution resulted in higher velocity ranges than the sequences with low temporal resolution. For the longitudinal velocity ranges, this difference was significant (P value ≤ 0.05). The global minimum is detected with all five sequences $DS^{n_{DS}}$, $AS^{n_{DS}}$, $AS^{n_{AS}}$, $RF^{n_{DS}}$ and $RF^{n_{AS}}$. The radial and longitudinal local minimum at

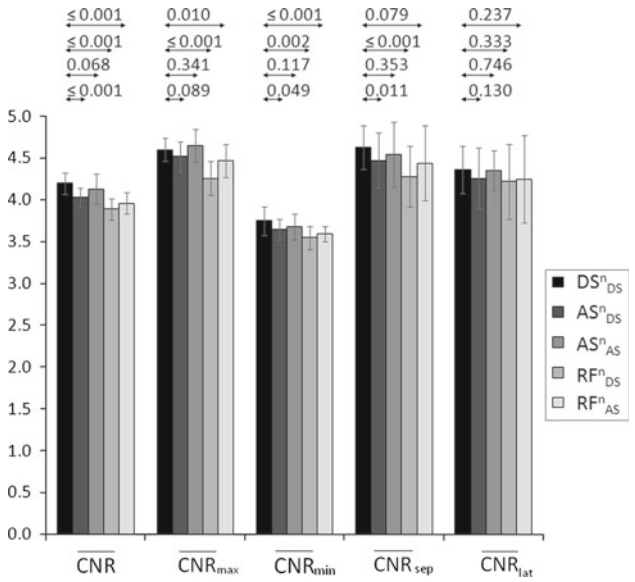

Fig. 3 CNR evaluation for all investigated sequences. CNR evaluation for all investigated sequences $DS^{n_{DS}}$, $AS^{n_{DS}}$, $AS^{n_{AS}}$, $RF^{n_{DS}}$ and $RF^{n_{AS}}$ over all volunteers. *P*-values between $DS^{n_{DS}}$ and the other sequences are displayed on the top of the bar graph

end-systole during the isovolumetric relaxation (IVRT) is detected more often with the sequences with higher temporal resolution. The percentages of detected radial and longitudinal local minima $P_{\text{local},r}$ and $P_{\text{local},l}$ are listed in Table 2. For all sequences, the radial local minimum is better detected than the longitudinal.

Discussion

A substantial reduction of the specific absorption rate and thus increased temporal resolution in black-blood cine TPM can be achieved by applying alternating presaturation pulses as well as by reduction of the flip angle. Both methods allow to acquire more heart phases in cases where the maximal number of heart phases is SAR limited. For all investigated approaches the achievable $\overline{\text{CNR}}$ between myocardium and blood pool appears reduced. In the case of alternating presaturation with maximum heart phases, a nonsignificant reduction was observed. All other investigated techniques showed a significant reduction. For all sequences the blood-

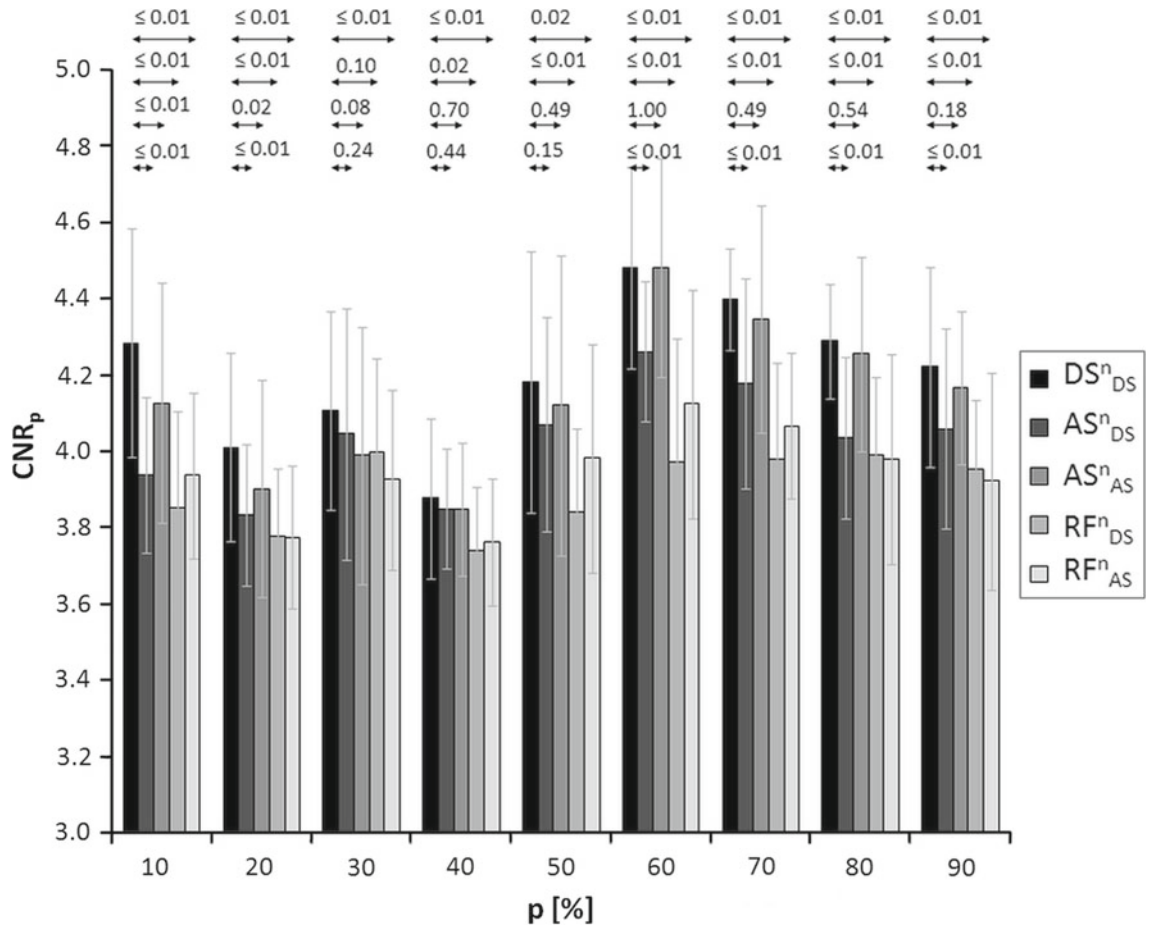

Fig. 4 CNR_p values for all investigated sequences and their respective *P* values. CNR_p is displayed for different percentages p of the RR-cycle for all investigated sequences. *P*-values between $DS^{n_{DS}}$ and the other sequences are displayed on the top of the bar graph

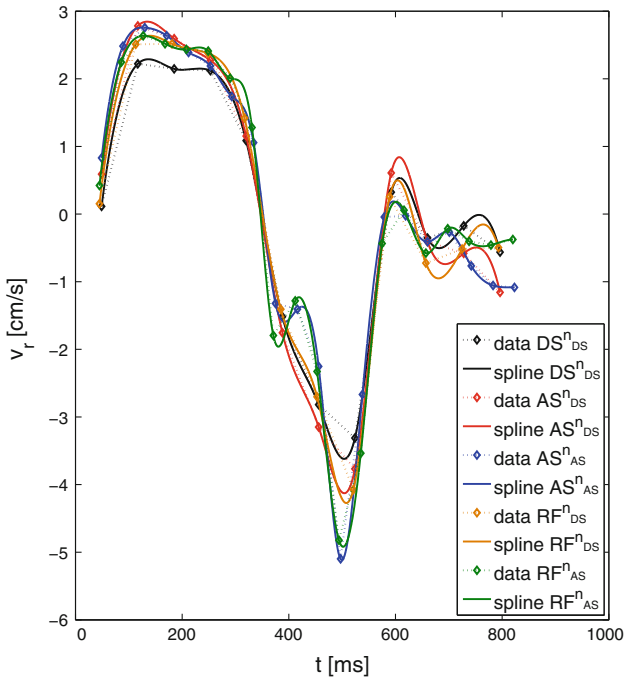

Fig. 5 Radial velocities over time for all investigated sequences exemplary for one volunteer. Radial velocities over time for all five investigated sequences $DS^{n_{DS}}$, $AS^{n_{DS}}$, $AS^{n_{AS}}$, $RF^{n_{DS}}$ and $RF^{n_{AS}}$ exemplary for one volunteer. High correlations could be observed for all velocity profiles. The low temporal resolution sequences show slightly reduced diastolic peak velocities. The velocity profiles obtained with high temporal resolution reveal more details

myocardium border could be delineated and flow-related artifacts were sufficiently suppressed. If SAR reduction is required for black-blood cine imaging the application of alternating presaturation pulses appears superior to a simple reduction of the flip angle.

For all investigated sequences, no significant $\overline{\text{CNR}}$ reduction compared to $DS^{n_{DS}}$ was obtained in the lateral wall. For the sequences $AS^{n_{DS}}$ and $RF^{n_{DS}}$, the septal wall shows significant $\overline{\text{CNR}}$ reductions. The spatial analysis of $\overline{\text{CNR}}$ therefore reveals, that $AS^{n_{AS}}$ and $RF^{n_{AS}}$ can be used without any local decrease in $\overline{\text{CNR}}$.

Temporally, the saturation effects vary similar in all investigated sequences and show less CNR during the end of systole. This might be explained by less blood exchange during this part of RR-cycle. At most time points, the sequence $AS^{n_{AS}}$ results in similar blood suppression than $DS^{n_{DS}}$ and performs superior than a reduction of flip angle. The results of $\overline{\text{CNR}}$ are therefore similar to the results of CNR_p.

No relevant difference in the low temporal resolution velocity profiles was observed. However, the velocity profiles acquired with improved temporal resolution revealed more details of the myocardial motion causing slightly reduced correlation coefficients $r(DS^{n_{DS}}, AS^{n_{AS}})$ and $r(DS^{n_{DS}}, RF^{n_{AS}})$. Additionally, higher velocity ranges were obtained with higher temporal resolution thus indicating a superior performance of $AS^{n_{AS}}$ and $RF^{n_{AS}}$. A similar observation regarding the influence of temporal resolution on the peak values was made by Jung et al. previously [22,23].

In [22] two main minima are detected in the equatorial slice with high temporal resolution (16.9 ms). In this study, the global minimum is detected with all investigated sequences, whereas the local minimum at end-systole at isovolumetric relaxation is more often detected with the sequences providing higher temporal resolution $AS^{n_{AS}}$ and $RF^{n_{AS}}$. This clearly indicates the need for SAR reduction at 3T for ensuring sufficient detail in the velocity curves.

To obtain high temporal resolution TPM data is important for providing similar temporal motion information when compared to tagging data [33], which has a temporal resolution of 20–40 ms, but an inferior spatial resolution (4–8 mm) than TPM (1–3 mm). One method to acquire even more cardiac phases would be the measurement of only 2 or 1 k-lines per segment. To compensate for the resulting long acquisition times, acceleration techniques such as kt-SENSE will likely be required.

By even further reducing the flip angle of the presaturation pulses to less than 37° the frame duration could be further reduced. However, the concomitant further reduction of $\overline{\text{CNR}}$ will limit the application of automatically segmentation.

Another method to further increase the temporal resolution is a combination of the introduced modified presaturation TPM sequences with view sharing [34,35], which reuses some of the same k-space data for the reconstruction of two ore more images [36].

To further improve the contrast, the location of the presaturation pulse may be controlled by the main flow direction. More basal presaturation pulses may be used during the

Table 2 Δv and P_{local} for all sequences and r(seq. x, seq. y) between $DS^{n_{DS}}$ and all other sequences averaged over all volunteers

Seq.	Δv_r	Δv_l	$P_{\text{local},r}$	$P_{\text{local},l}$	$r(DS^{n_{DS}}, \text{seq.})_r$	$r(DS^{n_{DS}}, \text{seq.})_l$
$DS^{n_{DS}}$	7.36 ± 1.03	14.16 ± 3.18	0.38	0.08		
$AS^{n_{DS}}$	7.52 ± 0.87	14.34 ± 2.81	0.62	0.00	0.99 ± 0.01	0.98 ± 0.02
$AS^{n_{AS}}$	7.94 ± 0.87	16.12 ± 2.58	0.85	0.38	0.97 ± 0.01	0.94 ± 0.03
$RF^{n_{DS}}$	7.64 ± 1.07	14.19 ± 2.98	0.46	0.00	0.98 ± 0.02	0.97 ± 0.03
$RF^{n_{AS}}$	7.85 ± 0.91	16.66 ± 2.44	0.77	0.69	0.96 ± 0.02	0.95 ± 0.02

filling phases and more apical presaturation pulses during contraction. For this process the exact systolic and diastolic timing must be known. This can be either done by a functional prescan, where the systolic and diastolic cardiac phases can be assessed, or by a previous quantitative measurement of through plane blood flow in the desired slice, using the information of the direction of inflow to place the presaturation pulse for each heart phase. This refined method would ensure saturation of spins likely entering the imaged slice. However, changes in the contraction pattern of the heart between prescan and TPM measurement may lead to unpredictable blood suppression in the corresponding heart phases.

In this study only short-axis views were acquired. The sequences investigated above could also be applied to long axis oriented cardiac views, however due to the reduced blood exchange in the long axis planes we assume, that the CNR would be decreased compared to the short-axis views.

Furthermore, in this study, only healthy volunteers have been investigated. In patients, limitations of the proposed techniques may rise in cases of reduced cardiac output causing insufficient blood exchange.

The application of the proposed techniques is also of interest for non-TPM applications such as a reduction of the field of view by spatial presaturation at high field strengths.

Conclusion

Black-blood cine TPM imaging at 3T with increased temporal resolution appears feasible with both investigated SAR reduction techniques. The application of alternating presaturation pulses leads to superior CNR values compared to spatial presaturation with reduced flip angle. The gain in CNR is almost independent on the location on the myocardium or the cardiac phase. The analysis of the myocardial motion obtained by the different sequences reveals that the achievable temporal resolution without SAR reduction is not sufficient to reveal all motion information. Therefore, SAR reduction for improved temporal resolution at 3T is desirable. The high temporal resolution sequences with either alternating saturation pulses or saturation pulses with reduced flip angle reveal higher peak velocities and a more detailed motion patterns. This gain of motion information might be of importance for myocardial motion analysis of patients with contraction abnormalities.

References

1. Drangova M, Zhu Y, Pelc NJ (1997) Effect of artifacts due to flowing blood on the reproducibility of phase-contrast measurements of myocardial motion. J Magn Reson Med 7:664–668
2. Felmlee J, Ehman R (1987) Spatial presaturation: a method for suppressing flow artifacts and improving depiction of vascular anatomy in MR imaging. Radiology 164:559–564
3. Delfino JG, Johnson KR, Eisner RL, Eder S, Leon AR, Oshinski JN (2008) Three-directional myocardial Phase-Contrast tissue velocity MR imaging with Navigator-Echo gating: in vivo and in vitro study. Radiology 246:917–925
4. Jung B, Schneider B, Markl M, Saurbier B, Geibel A, Hennig J (2004) Measurement of left ventricular velocities: phase contrast MRI velocity mapping versus tissue-doppler-ultrasound in healthy volunteers. J Cardiovasc Magn Reson 6:777–783
5. Petersen SE, Jung BA, Wiesmann F, Selvanayagam JB, Francis JM, Hennig J, Neubauer S, Robson MD (2006) Myocardial tissue phase mapping with cine phase-contrast mr imaging: regional wall motion analysis in healthy volunteers. Radiology 238:816–826
6. Nayak KS, Rivas PA, Pauly JM, Scott GC, Kerr AB, Hu BS, Nishimura DG (2001) Real-time black-blood MRI using spatial presaturation. J Magn Reson Med 13:807–812
7. Hennig J, Schneider B, Peschl S, Markl M, Laubenberger TKJ (1998) Analysis of myocardial motion based on velocity measurements with a black blood prepared segmented gradient-echo sequence: Methodology and applications to normal volunteers and patients. J Magn Reson Med 8:868–877
8. Bradley WG (1988) Carmen lecture. Flow phenomena in MR imaging. Am J Roentgenol 150:983–994
9. Mayo J, Culham J, MacKay A, Aikins D (1989) Blood MR signal suppression by preexcitation with inverting pulses. Radiology 173:269–271
10. Edelman R, Chien D, Kim D (1991) Fast selective black blood MR imaging. Radiology 181:655–660
11. Reichenbach JR, Venkatesan R, Schillinger DJ, Kido DK, Haacke EM (1997) Small vessels in the human brain: MR venography with deoxyhemoglobin as an intrinsic contrast agent. Radiology 204:272–277
12. Frahm J, Merboldt KD, Hanicke W, Haase A (1985) Stimulated echo imaging. J Magn Reson Med 64:81–93
13. Frahm J, Hanicke W, Bruhn H, Gyngell ML, Merboldt KD (1991) High-speed STEAM MRI of the human heart. Magn Reson Med 22:133–142
14. Fahmy AS, Pan L, Stuber M, Osman NF (2006) Correction of through-plane deformation artifacts in stimulated echo acquisition mode cardiac imaging. Magn Reson Med 55:404–412
15. Basha TA, Ibrahim EH, Weiss RG, Osman NF (2009) Cine cardiac imaging using black-blood steady-state free precession (BB-SSFP) at 3T. J Magn Reson Med 30:94–103
16. Koktzoglou I, Li D (2007) Diffusion-prepared segmented steady-state free precession: application to 3D black-blood cardiovascular magnetic resonance of the thoracic aorta and carotid artery walls. J Cardiovasc Magn Reson 9:33–42
17. Sirol M, Itskovich VV, Mani V, Aguinaldo JGS, Fallon JT, Misselwitz B, Weinmann H, Fuster V, Toussaint J, Fayad ZA (2004) Lipid-rich atherosclerotic plaques detected by gadofluorine-enhanced in vivo magnetic resonance imaging. Circulation 109:2890–2896
18. Pell GS, Lewis DP, Branch CA (2003) Pulsed arterial spin labeling using TurboFLASH with suppression of intravascular signal. Magn Reson Med 49:341–350
19. Bornstedt A, Bernhardt P, Hombach V, Kamenz J, Spiess J, Subgang A, Rasche V (2008) Local excitation black blood imaging at 3T: application to the carotid artery wall. Magn Reson Med 59:1207–1211
20. Miller S, Simonetti OP, Carr J, Kramer U, Finn JP (2002) MR imaging of the heart with cine true fast imaging with steady-state precession: influence of spatial and temporal resolutions on left ventricular functional parameters. Radiology 223:263–269

21. Inoue Y, Nomura Y, Nakaoka T, Watanabe M, Kiryu S, Okubo T, Ohtomo K (2005) Effect of temporal resolution on the estimation of left ventricular function by cardiac MR imaging. Magn Reson Imaging 23:641–645
22. Jung B, Föll D, Böttler P, Petersen S, Hennig J, Markl M (2006) Detailed analysis of myocardial motion in volunteers and patients using high-temporal-resolution MR tissue phase mapping. J Magn Reson Imaging 24:1033–1039
23. Jung B, Zaitsev M, Hennig J, Markl M (2006) Navigator gated high temporal resolution tissue phase mapping of myocardial motion. Magn Reson Med 55:937–942
24. Haacke EM, Brown RW, Thompson MR, Venkatesan R (1999) Magnetic resonance imaging: physical principles and sequence design. Wiley, New York
25. Pelc NJ, Bernstein MA, Shimakawa A, Glover GH (1991) Encoding strategies for three-direction phase-contrast MR imaging of flow. J Magn Reson Imaging 1:405–413
26. Souza SP, Szumowski J, Dumoulin CL, Plewes DP, Glover G (1988) SIMA: simultaneous multislice acquisition of MR images by hadamard-encoded excitation. J Comput Assist Tomogr 12:1026–1030
27. Delfino JG, Bhasin M, Cole R, Eisner RL, Merlino J, Leon AR, Oshinski JN (2006) Comparison of myocardial velocities obtained with magnetic resonance phase velocity mapping and tissue doppler imaging in normal subjects and patients with left ventricular dyssynchrony. J Magn Reson Imaging 24:304–311
28. Wang Y, Rossman PJ, Grimm RC, Riederer SJ, Ehman RL (1996) Navigator-echo-based real-time respiratory gating and triggering for reduction of respiration effects in three-dimensional coronary MR angiography. Radiology 198:55–60
29. Bellenger NG, Gatehouse PD, Rajappan K, Keegan J, Firmin DN, Pennell DJ (2000) Left ventricular quantification in heart failure by cardiovascular MR using prospective respiratory navigator gating: comparison with breath-hold acquisition. J Magn Reson Imaging 11:411–417
30. Fradkin M, Ciofolo C, Mory B, Hautvast G, Breeuwer M (2008) Comprehensive segmentation of cine cardiac mr images. In: Metaxas DN, Axel L, Fichtinger G, Székely G (eds) MICCAI (1), vol 5241 of Lecture Notes in Computer Science. Springer, pp 178–185
31. Hautvast G, Lobregt S, Breeuwer M, Gerritsen F (2006) Automatic contour propagation in cine cardiac magnetic resonance images. IEEE Trans Med Imaging 25:1472–1482
32. Walker PG, Cranney GB, Scheidegger MB, Waseleski G, Pohost GM, Yoganathan AP (1993) Semiautomated method for noise reduction and background phase error correction in MR phase velocity data. J Magn Reson Imaging 3:521–530
33. Zerhouni EA, Parish DM, Rogers WJ, Yang A, Shapiro EP (1988) Human heart: tagging with MR imaging—a method for noninvasive assessment of myocardial motion. Radiology 169:59–63
34. Foo TK, Bernstein MA, Aisen AM, Hernandez RJ, Collick BD, Bernstein T (1995) Improved ejection fraction and flow velocity estimates with use of view sharing and uniform repetition time excitation with fast cardiac techniques. Radiology 195:471–478
35. Markl M, Hennig J (2001) Phase contrast MRI with improved temporal resolution by view sharing: k-space related velocity mapping properties. Magn Reson Imaging 19:669–676
36. Bernstein MA, King KF, Zhou XJ (2004) Handbook of MRI pulse sequences. Elsevier Academic Press, Amsterdam